Materials Science and Engineering B 174 (2010) 216–221

Contents lists available at ScienceDirect

Materials Science and Engineering B

journal homepage: www.elsevier.com/locate/mseb

Structural studies of mechano-chemically synthesized $CuIn_{1-x}Ga_xSe_2$ nanoparticles

B. Vidhya [a,*], S. Velumani [a], Jesus A. Arenas-Alatorre [b], Arturo Morales-Acevedo [a], R. Asomoza [a], J.A. Chavez-Carvayar [c]

[a] Department of Electrical Engineering, SEES, CINVESTAV-IPN, Mexico, D.F., C.P. 07360, Mexico
[b] Institute of Physics, Universidad Nacional Autónoma de México, A.P. 20-364, 01000 México, D.F., Mexico
[c] Instituto de investigaciones en Materiales, UNAM, Mexico, D.F., Mexico

ARTICLE INFO

Article history:
Received 8 September 2009
Received in revised form 4 February 2010
Accepted 5 March 2010

Keywords:
CIGS
Ball milling
XRD
HRTEM
SAED

ABSTRACT

$CuInGaSe_2$ is a I–III–VI_2 semiconducting material of tetragonal chalcopyrite structure. It is a very prominent absorber layer for photovoltaic devices. Particle-based coating process for CIGS is considered to be promising technique with relatively simple procedures and low initial investment. In the present work CIGS nanoparticle precursors suitable for screen-printing ink has been prepared by ball milling. High purity elemental copper granules, selenium and indium powders and fine chips of gallium were used as starting materials. First the ball milling was carried out for $CuIn_{1-x}Ga_xSe_2$ ($x = 0.5$) with (i) 10 ml of ethyl alcohol (ii) 5 ml of tetra ethylene glycol (wet) and (iii) 1 ml of ethylene diamine (semi-dry) for a milling time of 3 h and the results are not stoichiometric. In order to obtain an improved stoichiometric composition dry ball milling of elemental sources for three different compositions of $CuIn_{1-x}Ga_xSe_2$ ($x = 0.25$, 0.5 and 0.75) has been carried out. X-ray diffraction analysis revealed the presence of (1 1 2), (2 2 0)/(2 0 4), (3 1 2)/(1 1 6), (4 0 0) and (3 3 2) reflections for all the milled powders. These reflections correspond to chalcopyrite structure of CIGS. Shift in peaks towards higher value of 2θ is observed with the increase in Ga composition. Average grain size calculated by Scherrer's formula is found to be around 13 nm for the dry samples milled for 1.5 h and 7–8 nm for the samples wet milled for 3 h. Lattice constants '*a*' and '*c*' are found to decrease with the increase in concentration of Gallium. FESEM analysis revealed a strong agglomeration of the particles and the particle size varied from 11 to 30 nm for the dry-milled samples. Composition of milled powders has been studied by energy dispersive X-ray analysis. TEM analysis revealed the presence of nanocrystalline particles and SAED pattern corresponds to (1 1 2), (2 2 0)/(2 0 4), (5 1 2)/(4 1 7) and (6 2 0)/(6 0 4) diffraction peaks of CIGS. From the HRTEM analysis the *d*-spacing values were evaluated and found to be 1.06, 3.33, 2.03 and 0.906 Å corresponding to the diffraction pattern. Also the planes corresponding to the nanoparticles have been simulated and matched with the HRTEM pattern. Raman spectra show the intense peak at 168–172 cm^{-1}, which corresponds to the chalcopyrite structure.

1. Introduction

Copper indium gallium diselenide (CIGS) is one of the few thin film materials presently being evaluated as an absorber layer in polycrystalline photovoltaic devices. CIGS is an alloy of two ternary semiconductors, $CuInSe_2$ and $CuGaSe_2$ with bandgap of 1.0 and 1.7 eV (at 300 K), respectively. The direct energy gap of CIGS results in a large optical absorption coefficient (10^5 cm^{-1}), which in turn permits the use of thin layers (1–2 μm) of active material [1,2] for device applications. CIGS photovoltaic (PV) cells are also known for their long-term stability [3]. Our interest lies in taking advantage of the benefits offered by nanotechnology to make inexpensive and efficient PV cells. Nano-structured layers in thin film solar cells offer three important advantages. First, due to multiple reflections, the effective optical path for absorption is much larger than the actual film thickness. Second, light generated electrons and holes need to travel over a much shorter path and thus recombination losses are greatly reduced. Third, the energy band gap of various layers can be tailored to the desired design value by varying the size of nanoparticles. This allows for more design flexibility in the absorber and window layers in the PV cell [4].

In recent years non-vacuum deposition techniques with a capability to prepare large area uniform thin films using low capital cost

* Corresponding author. Tel.: +52 55 5747 2036; fax: +52 55 5747 4003.
E-mail addresses: vidhyabhojan@gmail.com, vidhyabhojan@yahoo.co.in (B. Vidhya).

0921-5107/$ – see front matter © 2010 Elsevier B.V. All rights reserved.
doi:10.1016/j.mseb.2010.03.014

investment such as paste coating [5] and electrodeposition [6,7] has gained more attention among the researchers. Among the low cost processing techniques, nanoparticle-based coating process is considered to be promising as an alternative non-vacuum technique with relatively simple procedures and low initial investment [8]. Nanoparticle-based processes generally involves two step fabrication method, in which the synthesis of nanoparticles is followed by a non-vacuum coating method and then the precursor films are subjected to sintering to form an appropriate absorber layer for a PV cell [8,9]. In this process, major benefit comes from the nanosize effects of particles which lowers the melting point of the material [10], due to high surface energy and hence result in an exothermal reaction during sintering.

Commonly used methods for the synthesis of CIGS nanoparticles include solvothermal technique, low temperature colloidal synthesis [11,12]. Among them, solvothermal technique is time consuming, for example a reaction temperature of 280 °C for 36 h and then cooling to room temperature has been reported by Chun et al. [11]. Low temperature colloidal synthesis uses Na_2Se as one of the starting materials, which is highly toxic [12]. Thus, mechanochemical synthesis is considered as a suitable method which employs the elemental (Cu, In, Ga and Se) sources and a comparatively less time [13]. CIGS microparticles have been prepared by ball milling of elemental sources at 300 rpm [14]. CIGS powder prepared by ball milling have been screen printed to form PV cells with efficiency of 3.1% [15]. To the best of our knowledge there are only very few reports available on the preparation of CIGS nanoparticles by mechano-chemical synthesis. Also no matter what kind of methods are used to fabricate the nanoparticles, the nanoparticles will aggregate again because of the effects of Coulomb electrostatic force and Van der Waal force as soon as the grain size of the nanoparticles is smaller than 100 nm. In this situation, the nanoparticles do not show any significant size effect [16]. Recently, the wet-type milling has been used to produce the nanoparticles and avoid the aggregation effect [17,18]. Hence in the present work semi-dry, wet ball milled and dry-milled CIGS nanoparticles has been prepared with a milling speed of 1200 rpm. Also the effect of varying the Ga compositions (0.25, 0.5 and 0.75) has been studied. In this article we report on semi dry and wet-milling of CIGS, where we confirm the presence of secondary phases for semi-dry (with ethylenediamine) and wet milled (with tetra ethylene glycol). Pure CIGS phase has been observed for wet milled (with ethyl alcohol) and dry–milled nanoparticles with elemental sources. The X-ray diffractometer (XRD) and High Resolution Transmission Electron Microscopy (HRTEM) results have been verified by simulation of CIGS chalcopyrite structure and the different plane of orientations.

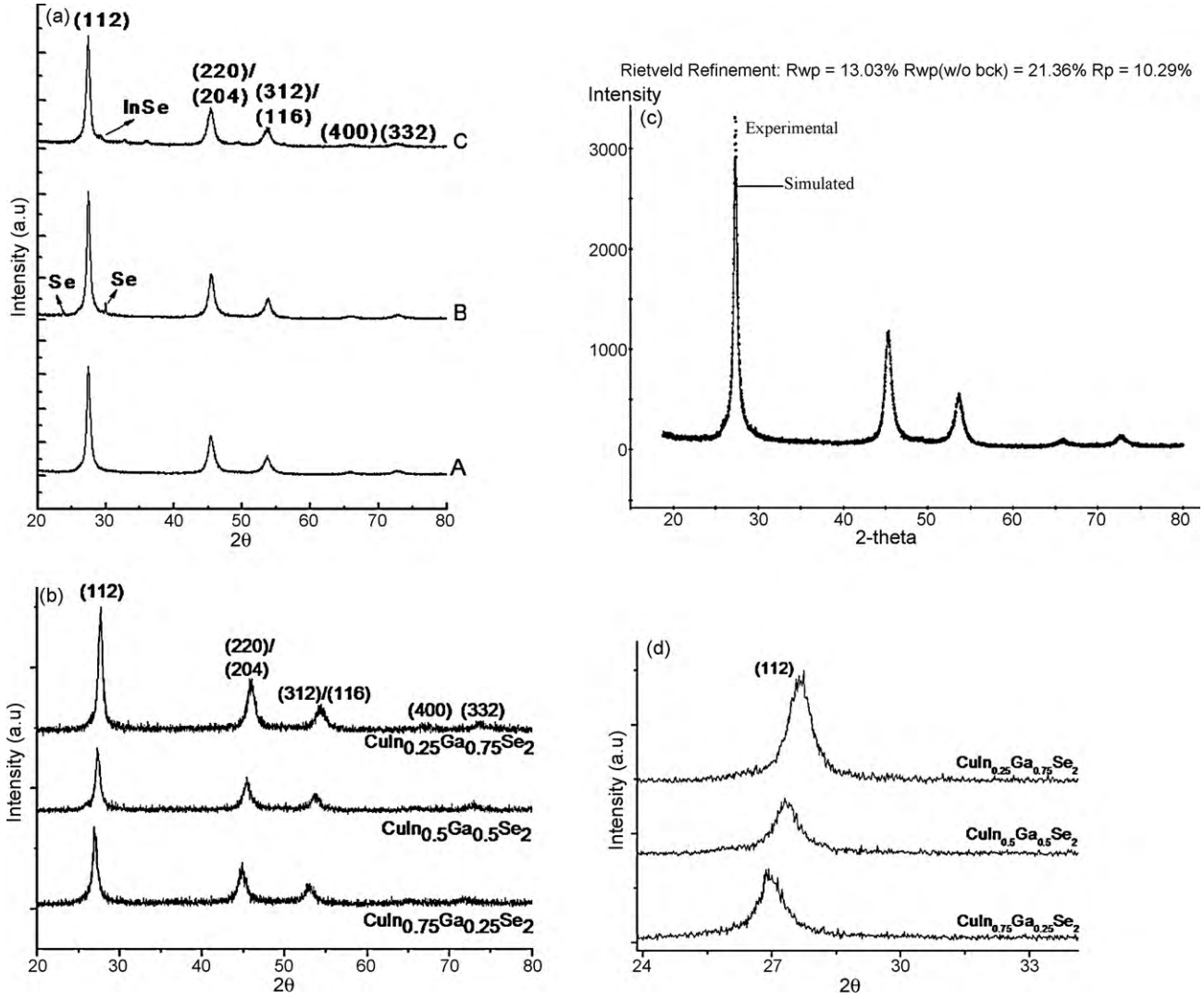

Fig. 1. (a) XRD pattern of wet milled CIGS nanoparticles (A) ethyl alcohol (B) tetra ethylene glycol(wet) and (C) ethylenediamine; (b) XRD pattern of ball milled CIGS nanoparticles; (c) experimental and simulated XRD pattern of $CuIn_{0.5}Ga_{0.5}Se_2$; (d) XRD pattern of d (1 1 2) region.

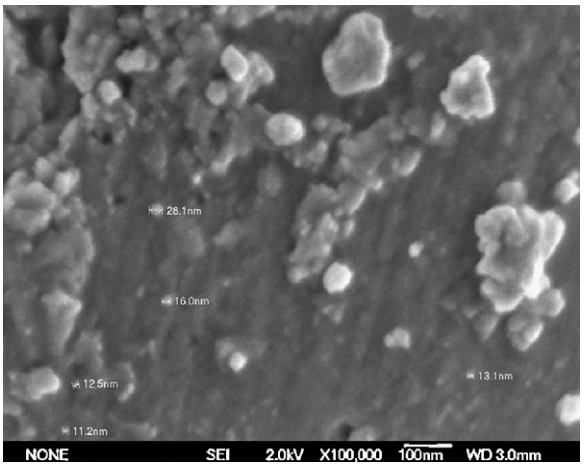

Fig. 2. FESEM analysis of $CuIn_{0.75}Ga_{0.25}Se_2$ nanoparticles.

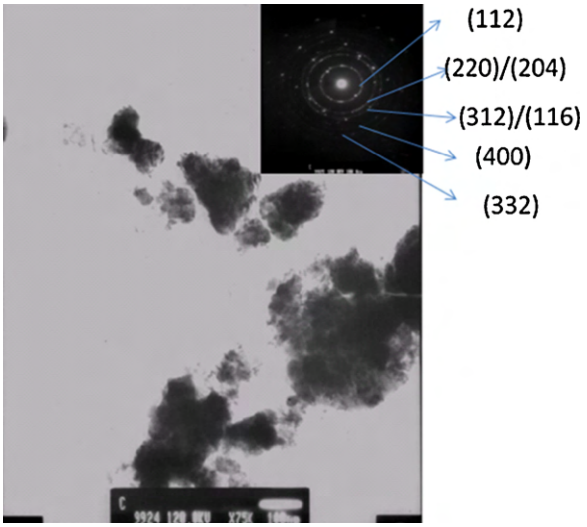

Fig. 3. TEM image of $CuIn_{0.5}Ga_{0.5}Se_2$ nanoparticles.

Table 1
Structural parameters of CIGS nanoparticles.

Sample	a (Å)	c (Å)	D (nm)	c/a	$u = 2\text{-}c/a$
$CuIn_{0.75}Ga_{0.25}Se_2$	5.70	11.49	12.24	2.015	−0.015
$CuIn_{0.5}Ga_{0.5}Se_2$	5.64	11.31	13.29	2.005	−0.005
$CuIn_{0.25}Ga_{0.75}Se_2$	5.57	11.22	13.96	2.014	−0.014

Table 2
Calculated texture coefficients.

(hkl)	(112)	(220)/(204)	(312)/(116)
$CuIn_{0.75}Ga_{0.25}Se_2$	0.9546	1.1939	0.8514
$CuIn_{0.5}Ga_{0.5}Se_2$	1.1210	0.8727	1.0062
$CuIn_{0.25}Ga_{0.75}Se_2$	1.0832	1.0425	0.8742

2. Experimental details

Starting materials, high purity elemental copper granules (>99.9% Sigma Aldrich), selenium and indium powders (>99.9% Aldrich) and fine chips of gallium (>99.99% Aldrich) were weighed to give $CuIn_{1-x}Ga_xSe_2$ (where $x = 0.5$). This blended elemental mixture and Stainless balls were loaded in a stainless container. In order to prevent oxidation of the powders, the weighing procedure was made in Argon gas atmosphere using a glove box. The ball-to-powder weight ratio was maintained at 10:1 and milling was carried out using a SPEX-8000 mixer/mill at 1200 rpm. First, milling of the $CuIn_{1-x}Ga_xSe_2$ with $x = 0.5$ has been carried out with (i) few ml of ethyl alcohol (wet), (ii) tetra ethylene glycol (wet) and (iii) with few drops of ethylene diamine (semi-dry) for 3 h. All the wet products were subjected to drying before analysis. Since the wet milled (tetra ethylene glycol) and semi-dry (ethylenediamine) samples showed the presence of secondary phases, dry milling of elemental sources has been carried out for three different compositions of Ga (0.25, 0.5 and 0.75).

Structure of the prepared nanoparticles were analyzed using an X-ray diffractometer (Siemens D5000, using Cu-Kα radiation with $\lambda = 1.5406$ Å). Measurements were made for 2θ values over 20–80°. Particle size of the prepared CIGS powders was analyzed by JEOL JSM-7401F Field Emission Scanning Electron Microscope (FESEM). Composition of the CIGS nanoparticle was analyzed by JEOL 840

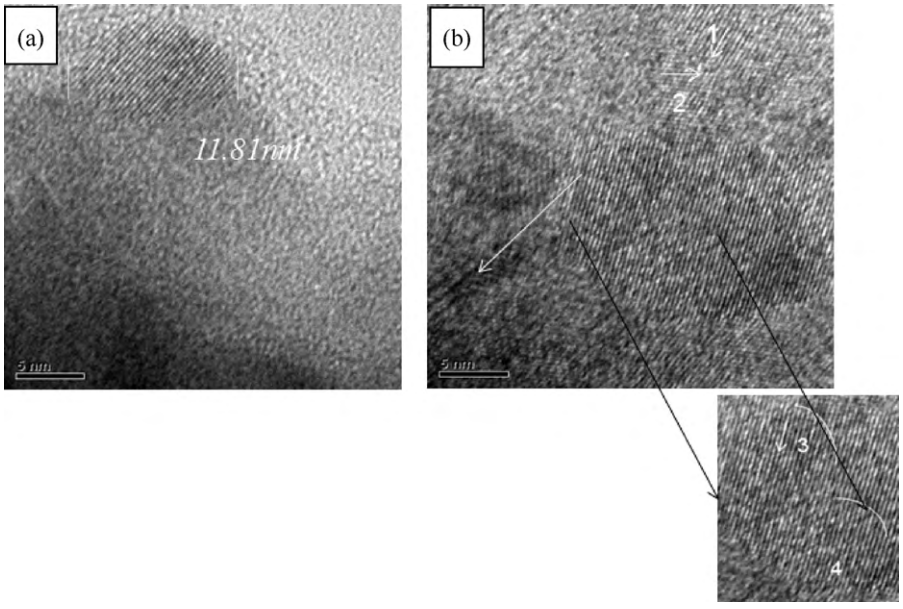

Fig. 4. HRTEM micrographs of $CuIn_{0.75}Ga_{0.25}Se_2$ prepared by mechano-chemical synthesis. (a) Identification of nanoparticle size around 11.81 nm and (b) example of fracture induced in the materials, strong aggregation of the nanoparticles and identification of particles 1, 2, 3 and 4.

SEM-energy dispersive X-ray analysis (EDS). TEM analysis were carried out by JEOL TEM 1200 EX. HRTEM analysis has been made using JEOL JEM 2010F. Micro Raman analysis is made using Horiba Jobin Yvan (Microscopy Olympus BX40) with He–Ne laser ($\lambda = 632$ nm).

3. Results and discussions

X-ray diffraction pattern of the nanoparticle powders prepared by wet and dry ball milling are shown in Fig. 1a and b, respectively. Main peaks appear corresponding to (1 1 2), (2 2 0)/(2 0 4), (3 1 2)/(1 1 6), (4 0 0) and (3 3 2) planes of the chalcopyrite structure [13,12]. Broadening of peaks is presumably due to the small size of particles [12]. It is also observed that wet-milling with ethyl alcohol produces pure CIGS without any secondary phases, whereas Tetra ethylene glycol creates a lattice distortion and separates the Se, which is evident from the peaks corresponding to Se as shown in Fig. 1a. Ball milling with ethylene diamine (semi-dry) leads to the formation of InSe binary phase. Dry-milled sample shows the presence of pure CIGS phase. For wet milled $CuIn_{1-x}Ga_xSe_2$ nanoparticles, atomic percentage of all the four elemental constituents Cu, In, Ga and Se vary in each sample, leading to non-stoichiometric composition which is not favorable for high efficiency PV applications. This is due to the reason that during the device fabrication, the surface treatment of CIGS absorber layer in Cd or Zn containing solution is shown to produce condition under which efficient solar cells can be fabricated [19]. During this process there is some inter-diffusion across the CdS/CIGS interface. Therefore CIGS films should have Cu/(In + Ga) <1, i.e. Cu poor and In + Ga rich, which would create an abundance of Cu vacancies at the interface. The ionic radii of Cu (0.070 nm) and Cd (0.097 nm) are very close and the substitution of Cd in Cu vacancy sites is most likely, and therefore the resulting composition mixing will reduce the effects of interface (CdS/CIGS) carrier recombination, thus leading to higher efficiency. Apart from this effect Sakurai et al. [20] have reported that the Cu/(In + Ga) affect the morphology of CIGS absorber layer. Similarly, Kaufamn et al. [21] have observed an increase in roughness of the film when Cu/(In + Ga) > 1. Based on these aspects the optimum value of Cu/(In + Ga) ranges from 0.8 to 0.95, which is less than 1 [22–24]. Here for both the wet milled samples Cu/(In + Ga) > 1, i.e. 1.017 and 1.096 for ethyl alcohol and terta ethylene glycol, respectively, which shows that these two compositions are not suitable for high efficiency PV applications [25]. Thus it can be confirmed that the chemicals added-(ethyl alcohol, tetra ethylene diamine and ethylene glycol) has a strong influence on the composition of the quaternary compound CIGS. Therefore further studies have been carried out only for dry-milled samples, varying the Ga composition (0.25, 0.5 and 0.75).

Chalcopyrite structure of $CuIn_{0.5}Ga_{0.5}Se_2$ has been simulated using the space group I42d (1 2 2) with the standard lattice constants $a = 5.673$ Å and $c = 11.322$ Å (JCPDS-40-1488) [26] and the experimental diffraction pattern is matched with the simulated pattern by Rietveld refinement, as shown in Fig. 1c. Apart from this for the samples with different Ga composition ($x = 0.25$, 0.5 and 0.75), the FWHM of peaks decreases with the increase in Ga; as an example, for (1 1 2) peak the FWHM values are 0.697°, 0.642° and 0.612° for $x = 0.25$, 0.5 and 0.75, respectively, this corresponds to an increase in the average grain size [27]. As gallium concentration increases, all signals shift towards larger diffraction angles; Fig. 1d shows this effect on the d (1 1 2) signal. Position of the peak corresponding to (1 1 2) orientation is found to shift to higher values of 2θ with the increase in Ga, i. e. from 26.88° for the composition $CuIn_{0.75}Ga_{0.25}Se_2$ to 27.28° for $CuIn_{0.5}Ga_{0.5}Se_2$ to 27.65° for $CuIn_{0.25}Ga_{0.75}Se_2$. This noticeable shift is due to the decrease in lattice constants '*a*' and '*c*' as reported by Olejnicek [28].

Lattice parameters '*a*' and '*c*' for the tetragonal system are calculated from:

$$\frac{1}{d^2} = \frac{h^2 + k^2}{a^2} + \frac{l^2}{c^2} \quad (1)$$

As given in Table 2, the lattice parameter values '*a*' and '*c*' are found to decrease as Ga concentration increases and this is due to the small ionic size of Ga (0.62 Å) compared to In (0.81 Å) and hence causes shrinkage of the lattice as they substitute in sites in the cell.

Table 1 gives the value of c/a and hence the lattice distortion u, which shows that the prepared CIGS nanoparticles are very close to the ideal tetragonal structure for which $c/a = 2$ [29]. $CuIn_{0.5}Ga_{0.5}Se_2$ shows comparatively less distortion than the other two composi-

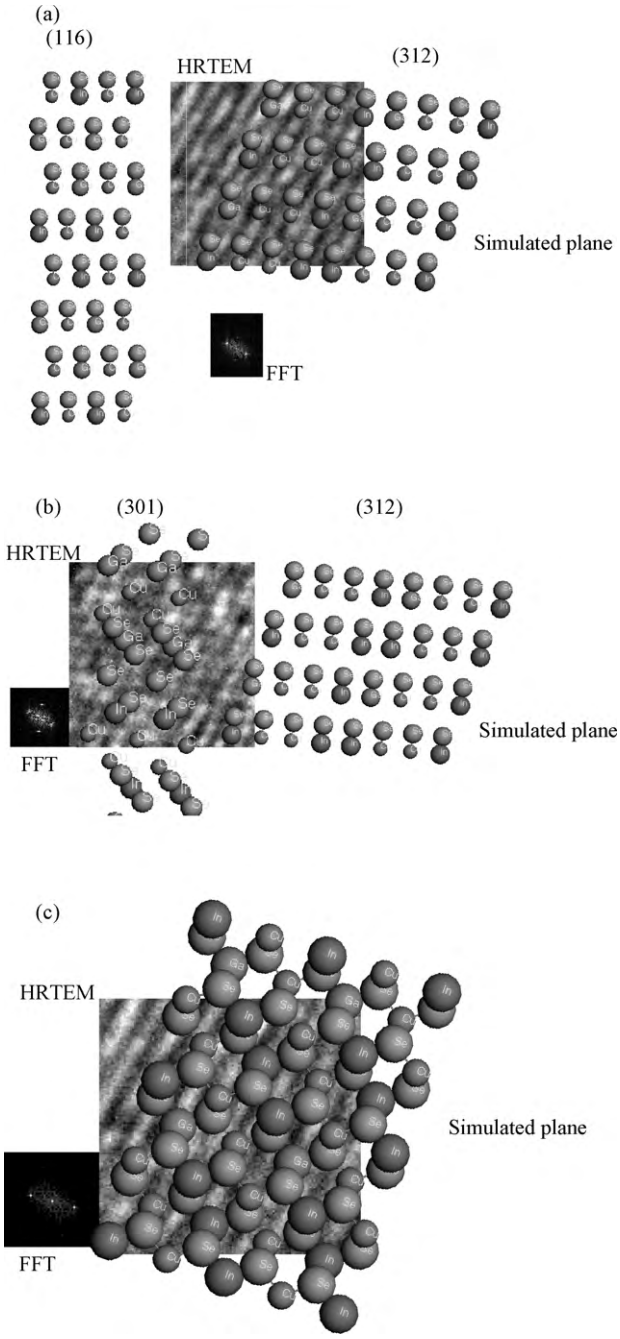

Fig. 5. Matching of the experimental HRTEM pattern with the simulated crystal planes for particle 1, 2 and 3 marked in Fig. 4b. Simulated plane. (a) Nanoparticle 1, *d*-spacing 1.72 Å; (b) nanoparticle 2, *d*-spacing 1.88 Å—(3 0 1) and 1.713 Å—(3 1 2); (c) nanoparticle 3, *d*-spacing 2.04 Å—(2 2 0).

tions. A preferred orientation is observed along the (2 2 0)/(2 0 4) peak for $CuIn_{0.25}Ga_{0.75}Se_2$, but for higher composition of Ga the preferred orientation shifted to (1 1 2) peak, which is confirmed by the texture coefficient calculated from Eq. (2) and given in Table 2. Virtuani et al. [30] have reported that in the case of chalcopyrite CIGS thin films the strongest reflexions are the (1 1 2) and the overlapping (2 2 0)/(2 0 4), which corresponds to different preferred orientations.

$$\text{Texture coefficient} = \frac{I_{(h\ k\ l)}}{I_{0(h\ k\ l)}}\left[\frac{1}{n\sum_{i=1,\ldots,n} I_{(h\ k\ l)}/I_{0(h\ k\ l)}}\right]^{-1} \quad (2)$$

where $I_{(hkl)}$ is the experimental value obtained, $I_{0(hkl)}$ is the standard data and n is the number of peaks considered.

Grain size is calculated from Scherrer's formula and the values are listed in Table 1.

$$D = \frac{0.94\lambda}{\beta\cos\theta} \quad (3)$$

It is found that the grain size increases with the increase in Ga from 0.25 to 0.75, which is obvious from the decrease in FWHM as mentioned above.

FESEM analysis is carried out for $CuIn_{0.5}Ga_{0.5}Se_2$ sample. As shown in Fig. 2, a strong aggregation of particles is observed, where some separate nanoparticles of 11–30 nm have been identified. Composition analysis of the CIGS nanoparticle powders shows that for all the three compositions of Ga (0.25, 0.5 and 0.75), Cu/(In + Ga) <1 i.e. 0.927, 0.803, 0.851 and therefore near stoichiometric composition has been obtained. The standard deviation value of composition is found to be less than 2.

TEM was employed to further examine the crystal sizes of the product. As shown in Fig. 3, the TEM micrograph reveals an agglomerate of nanoparticles in which dark particles are surrounded by non-dense materials. At the same time, from the Selected Area Diffraction (SAED) pattern it can be observed that there is a good crystalline order, which is in agreement with the XRD results. Fine bright spots in the SAED pattern are related to the nanocrystalline phase of CIGS [27], here it should be noted that CIGS nanoparticles prepared by low temperature colloidal synthesis has resulted in a non-perfect crystalline structure, with broad and diffuse rings observed in the SAED pattern [12]. This confirms that good crystallinity is obtained by mechano-chemical synthesis.

HRTEM images allow the determination of size of the nanoparticles [31], the type of structures produced [32] and also the possible induced morphologies [33], so we used it to recognize these variables from our samples. In Fig. 4a, a single particle is clearly identified with the size of 11.81 nm; this confirms the value of 12.75 nm obtained from Scherrer's formula. HRTEM images allow finding defects in the nanocrystalline material as marked with a bigger arrow in Fig. 4b; these can be representatives of the processes that induce the reduction of nanocrystal size during mechano-chemical synthesis. Also Fig. 4b shows the strong aggregation of CIGS nanoparticles; here we have identified the different nanoparticles with the different direction of orientation as marked with arrows for each nanoparticle. Nanoparticle 1 gives the lattice spacing of 1.72 Å, which corresponds to the (1 1 6)/(3 1 2) planes, in order to confirm the best fit among these two planes, we have simulated the crystal planes of CIGS chalcopyrite structure and matched it with the HRTEM pattern. As shown in Fig. 5a the simulated (3 1 2) plane matches with the experimental result, thus confirming the orientation corresponding to this particular plane. Similarly the corresponding planes for nanoparticles 2 and 3 have been simulated and matched with the experimental pattern as shown in Fig. 5b and c. Nanoparticle 2 corresponds to two different planes (2 2 0) and (3 1 2) as is evident from the FFT. Both these planes have been simulated and presented in Fig. 5b. Thus we are able to strongly define the plane of orientation of the nanoparticles. Finally, in the inset of Fig. 6, Fast Fourier Transform (FFT) denotes a polycrystalline material, which must be composed of nanocrystals. The d-spacing corresponding to (1 1 2), (2 2 0)/(2 0 4), (3 1 2)/(4 1 7) and (6 2 0)/(6 0 4) diffraction peaks of CIGS has been observed, which again confirms the chalcopyrite structure of CIGS. The lattice parameters calculated from the HRTEM analysis for $CuIn_{0.5}Ga_{0.5}Se2$ gives $a = 5.741$ Å and $c = 11.66$ Å which is close to the calculated values from XRD result.

Fig. 7 shows that all the samples exhibit Raman spectra with single, intense scattering peak between 168 and 172 cm^{-1}, with the increase in Ga composition from 0.25 to 0.75, respectively, corresponding to the A1 optical phonon mode that is the characteristic of chalcopyrite crystal structures [12]. This is in agreement with a linear dependence of the frequency of A1 mode with the increase in Ga as reported by Papadimitriou et al. [34]. Also they have reported the A1 mode frequency of 172.4 cm^{-1} for small Ga composition ($x = 8.0\%$). In our case the sample with 168 cm^{-1} has (7.22% Ga–EDX composition). Apart from this, Raman frequency is also affected due to the weakening of bond-stretching forces with the decrease in Cu content, which is observed in all our samples where Cu/(In + Ga) < 1, leading to the shift in low frequency compared to 172.4 cm^{-1} for $x = 8.0\%$ as discussed above. Also the FWHM values of 20.52, 11.84 and 10.79 cm^{-1} are determined for the samples with Cu/(In + Ga) corresponding to 0.92, 0.851 and 0.803, respectively. Similar trend

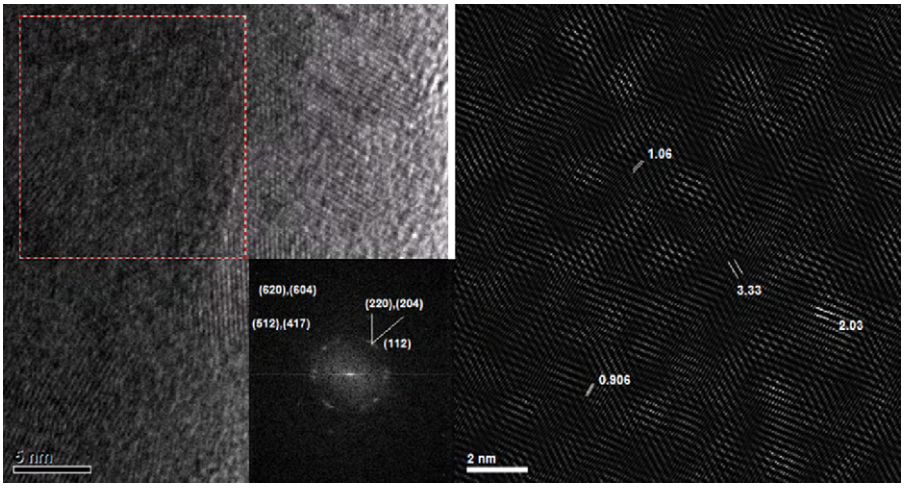

Fig. 6. HRTEM analysis, determination of structure with the help of interplanar distance measurement.

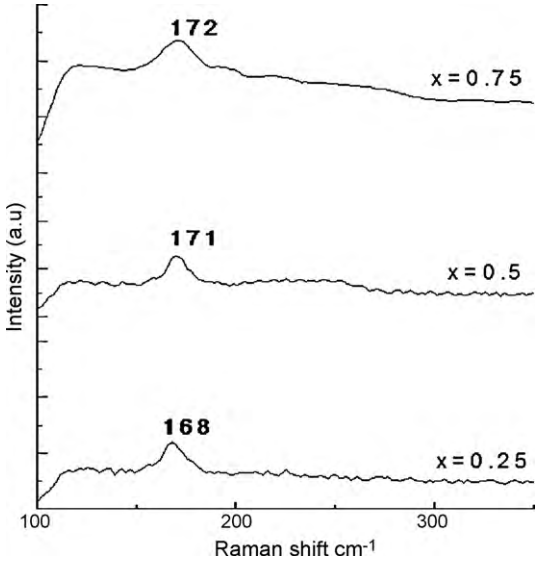

Fig. 7. Raman spectra of $CuIn_{1-x}Ga_xSe_2$ nanoparticles.

has been reporterd by Papadimitriou et al. [34] where they have observed the broadening of peaks with the decrease in Cu/(In) or (Ga) content for $CuInSe_2$ and $CuGaSe_2$. Therefore Raman analysis serves as a qualitative technique for determination of the composition of mechanochemically synthesized $CuInGaSe_2$ nanoparticles, which is in agreement with the EDX-composition analysis.

4. Conclusions

CIGS nanoparticles have been prepared by mechano-chemical synthesis. XRD result shows the chalcopyrite structure of CIGS. Ball milling with ethyl alcohol, tetra ethylene glycol and ethylenediamine has resulted in the formation of non-stoichiometric CIGS nanoparticles with the presence of secondary phases. The effect of Ga composition on the structural properties of ball milled CIGS nanoparticles has been studied. Decrease in lattice constants has been observed with the increase in Ga concentration. Nanostructure of particles is revealed by the broad XRD peaks. Change in preferred orientation from [2 2 0] to [1 1 2] has been observed with the increase in Ga. Aggregation of nanoparticles is observed in the FESEM analysis. TEM results confirm the presence of nanoparticles. HRTEM micrographs also confirm the aggregation of nanoparticles. Different direction of orientation of the nanoparticles has been confirmed by simulation of the corresponding crystal planes and matching with the HRTEM pattern. Raman studies indicate the shift in peak towards higher value with the increase in Ga. Thus CIGS nanoparticles can be prepared by an inexpensive technique via ball milling, further optimization of the milling speed and time may reduce the strong aggregation between particles and form well dispersed CIGS nanoparticles. Wet-milling with ethylenediamine and semi-dry with terta ethylene gylcol does not support the formation of pure single phase CIGS. Relative Ga composition $x = Ga/(In + Ga)$ affects the structural characteristics of the CIGS precursor powder. Thus we confirm that despite using a new process for the preparation of CIGS nanoparticles the material property is consistent. The prepared CIGS nanoparticle powder will be used to deposit CIGS films by screen-printing.

Acknowledgements

The authors would like to acknowledge Dr. Hector Calderón and his team of Escuela Superior de Fisica y Matematicas del IPN for providing the ball mill for sample preparation. We acknowledge the Solid State Physics group, Department of Physics, CINVESTAV for the XRD, FESEM and Raman analysis. We acknowledge Luis Rendón from IFUNAM for his technical help in HRTEM. We also acknowledge the contribution of Dr. Gaspar Casados-Cruz for making the SEM-EDX measurements. One of the authors B. Vidhya is thankful for the scholarship provided by CONACYT to pursue the Doctorate program.

References

[1] C. Chityuttakan, P. Chivetkitvanich, K. Yoodee, S. Chatraphron, Solar Energy Mater. Solar Cells 90 (2006) 3124–3129.
[2] D.B. Mitzi, M. Yuan, W. Liu, A.J. Kellock, S.J. Chey, L. Gignac, A.G. Schrott, Thin Solid Films 517 (2009) 2158–2162.
[3] J.F. Guillemoles, Thin Solid Films 403–404 (2002) 405–409.
[4] K.B. Jinesh, C. Sudha Kartha, K.P. Vijayakumar, Appl. Surf. Sci. 195 (2002) 263–269.
[5] J.W. Park, Y.W. Choi, E. Lee, S. Yoon, B.K. Min, J. Cryst. Growth 311 (2009) 2621–2625.
[6] R.N. Battacharya, W. Batchelor, J.E. Granata, F. Hasoon, H. Wiesner, K. Ramanathan, J. Keane, R.N. Noufi, Solar Energy Mater. Solar Cells 55 (1998) 83–94.
[7] K. Bouabid, A. Ihlal, A. Manar, A. Outzourhit, E.L. Ameziane, J. Phys. IV Fr. 123 (2005) 53–57.
[8] M. Kaelin, D. Rudmann, A.N. Tiwari, Low cost processing of CIGS thin film solar cells, Solar Energy 77 (2004) 749–756.
[9] S.J. Ahn, K.H. Kim, K.H. Yoon, Curr. Appl. Phys. 8 (2008) 766–769.
[10] S.J. Ahn, C.W. Kim, J.H. Yun, J.C. Lee, K.H. Yoon, Solar Energy Mater. Solar Cells 91 (2007) 1836–1841.
[11] Y.G. Chun, K.-H. Kim, K.-H. Yoon, Thin Solid Films 480–481 (2005) 46–49.
[12] S.J. Ahn, K.H. Kim, Y.G. Chun, K.H. Yoon, Thin Solid Films 515 (2007) 4036–4040.
[13] C. Suryanarayana, S.H. Yoo, J.R. Groza, J. Mater. Sci. Lett. 20 (2001) 2179–2181.
[14] T. Wada, Y. Matsuo, S. Nomura, Y. Nakamura, A. Miyamura, Y. Chiba, A. Yamada, M. Konagai, Phys. Status Solidi (a) 203 (2006) 2593–2597.
[15] J. Kubo, Y. Matsuo, T. Wada, A. Yamada, M. Konagai, Mater. Res. Soc. 1165 (2009) M05–13.
[16] Z.A. Peng, X.G. Peng, J. Am. Chem. Soc. 130 (49) (2008) 16770–16777.
[17] C. Frances, Powder Technol. 143 (2004) 253–263.
[18] C. Suryanarayana, Prog. Mater. Sci. 46 (2001) 1–184.
[19] K. Ramanathan, F.S. Hasooon, S. Smith, D.L. Young, M.A. Contreras, 13th ICTMC, October 14–18, 2002, pp. 1–4.
[20] K. Sakurai, R. Hunger, N. Tsuchimochi, T. Baba, K. Matsubara, P. Fons, A. Yamada, T. Kojima, T. Deguchi, H. Nakanishi, S. Niki, Thin Solid Films 431–432 (2003) 6–10.
[21] C.A. Kaufamn, A. Neisser, R. Klenk, R. Scheer, Thin Solid Films 480–481 (2005) 515–519.
[22] Chanwit Chityuttakan, Panita Chinvetkitvanich, Kajornyod Yoodee, Somphong Chatraphorn, Solar Energy Mater. Solar Cells 90 (2006) 3124–3129.
[23] M. Nouiri, Z. Ben Ayadi, K. Khirouni, S. Alaya, K. Djessas, S. Yapi, Mater. Sci. Eng. C 27 (2007) 1002–1006.
[24] A. Miguel, K. Contreras, J. Ramanathan, F. AbuShama, D.L. Hasoon, B. Young, R. Egaas, Noufi, Prog. Photovoltaics: Res. Appl. 13 (2005) 209–216.
[25] K. Ramanathan, J. Keane, R. Noufi, 31st IEEE Photovoltaics, January 3–7, 2005, NREL/CP-520-37404.
[26] D. Suri, K. Nagpal, G. Chadha, J. Appl. Crystallogr. 22 (1989) 578.
[27] F.B. Dejene, V. Alberts, J. Phys. D: Appl. Phys. 38 (2005) 22–25.
[28] J. Olejnicek, C.A. Kamler, A. Mirasano, A.L. Martinez-Skinner, M.A. Ingersoll, C.L. Exstrom, S.A. Darveau, J.L. Huguenin-Love, M. Diaz, N.J. Ianno, R.J. Soukup, Solar Energy Mater, Solar Cells 94 (2010) 8–11.
[29] M.R. Balboul, H.W. Schock, S.A. Fayak, A.A. El-Aal, J.H. Werner, A.A. Ramadan, Appl. Phys. A 92 (2008) 557–563.
[30] A. Virtuani, E. Lotter, M. Powallia, J. Appl. Phys. 99 (2006) 014906.
[31] M. Jose-Yacaman, J.A. Ascencio, H. Liu, J. Vacuum Sci. Technol. B 19 (2001) 1091–1107.
[32] J.A. Asencio, C. Gutierrez-Wing, M.E. Espinsa-Pesqueria, M. Marin, S. Tehuacanero, C. Zorrilla, M. Jose-Yacaman, Surf. Sci. 396 (1998) 349–369.
[33] J.A. Ascencio, H.B. Liu, U. Pal, A. Medina, Z.L. Wang, Microsc. Res. Tech. 69 (2006) 522–530.
[34] D. Papadimitriou, N. Esser, C. Xue, Phys. Stat. Sol. (b) 242 (2005) 2633–2643.